JOURNAL OF GEOPHYSICAL RESEARCH, VOL. 103, NO. C12, PAGES 27,621–27,635, NOVEMBER 15, 1998

Simulation of heat storages and associated heat budgets in the Pacific Ocean 2. Interdecadal timescale

Guillermo Auad, Arthur J. Miller, and Warren B. White

Climate Research Division, Scripps Institution of Oceanography, University of California, San Diego, La Jolla

Abstract. We use a primitive equation isopycnal model of the Pacific Ocean to simulate and diagnose the anomalous heat balance on interdecadal timescales associated with heat storage changes observed from 1970-1988 in the expendable bathythermograph (XBT) data set. Given the smallness of the interdecadal signals compared to the El Niño-Southern Oscillation (ENSO) signal, the agreement between model and observations is remarkably good. The total anomalous heat balance is made up of two parts, the diabatic part (from the model temperature equation) and the adiabatic part (from the model mass conservation equation) due to thermocline heave. We therefore describe our analysis of both the total and diabatic anomalous heat balances in four areas of the tropical and subtropical North Pacific Ocean in the upper 400 m. The interdecadal total (diabatic plus adiabatic) heat balance in the North Pacific Ocean is characterized by a complicated interplay of different physical processes, especially revealed in basin-scale averages of the heat budget components that have comparable amounts of variance. In smaller subregions, simpler balances hold. For example, in the western equatorial Pacific (area 1) the total heat content tendency term is nearly zero, so that a simple balance exists between surface heat flux, vertical heat transport, and horizontal mixing. In the western subtropical Pacific the total heat content tendency balances the three-dimensional divergence of the heat flux. We speculate that this complexity is indicative of multiple physical mechanisms involved in the generation of North Pacific interdecadal variability. The diabatic heat balance north of 24°N, a region of special interest to The World Ocean Circulation Experiment (WOCE), can be simplified to a balance between the tendency term, surface heat flux, and meridional advection, the last term dominated by anomalous advection of mean temperature gradients. For the western equatorial region the diabatic heat content tendency is nearly zero and the steady balance involves simply horizontal advection and the surface heat flux, which at these latitudes has a damping role in the model. An important finding of this study is the identification of two interdecadal timescales, roughly 10 and 20 years, both similar to those reported by other investigators in recent years. [*Tourre et al.,* 1998; *Latif and Barnett,* 1994; *Robertson,* 1995; *White et al.,* 1997; *Gu and Philander,* 1997; *Jacobs et al.,* 1994]. The 20-year timescale is only present in diabatic heat budget components, while the 10-year timescale is present in both diabatic and adiabatic components. The 10-year timescale can also be seen in the surface heat flux time series, but it occurs in the ocean adiabatic components which demonstrates the importance of oceanic adjustment through Rossby wave dynamics on decadal timescales.

1. Introduction

Owing to the scarcity of long records, interdecadal oceanic variability still remains largely unexplained. There are many hypotheses about the origin of this variability and one of the most important issues that still needs to be addressed is the degree to which oceanic variability, can be generated by the ocean itself, by the overlying atmospheric system or by feedbacks between the ocean-atmosphere system. A better understanding of this process is crucial to understanding the decadal climate variations that can affect humanity in many ways.

In the Pacific Ocean, several different ideas have been advanced that explain some aspects of its tropical and extratropical interdecadal variability. These ideas span

Paper number 98JC02064.
0148-0227/98/98JC-02064$09.00

the range of stocastically forced ocean systems [*Frankignoul et al.*, 1997; *Jin*, 1996], tropical forcing of midlatitude ocean variations [*Graham*, 1994; *Trenberth*, 1990], intrinsic midlatitude ocean-atmosphere interactions [*Latif and Barnett*, 1994; *Robertson*, 1995], and tropical-extratropical interacting systems [*Gu and Philander*, 1997; *Kirtman and Schopf*, 1997]. It is possible that more than one of these processes and forcing mechanisms are present, each acting in distinct (or overlapping) parts of the basin at different (or the same) times with different amplitude and different timescale. A variety of physical mechanisms acting simultaneously could explain the broadband nature of decadal-scale variations in the Pacific seen, e.g., in the heat storage empirical orthogonal functions (EOFs) computed from model results by *Latif and Barnett* [1994, 1996] and computed from observations by *Tourre et al.* [1998] that explain only about one third of the total variance in the interdecadal period band (low signal-to-noise ratio).

In this paper, we use data from an ocean general circulation model (OGCM) and temperature observations of the Pacific Ocean from 1970 to 1988 (19-year long records) to characterize interdecadal variability of upper ocean heat content (also called heat storage), which has obvious importance in climate feedbacks. Our plan is to identify the physical mechanisms that cause heat content to vary in different parts of the Pacific so that these mechanisms can eventually help to distinguish which theories of interdecadal variability, most of them mentioned above, are most consistent with observations. We distinguish between diabatic and adiabatic changes in heat content in order to better understand the processes involved. A process is called adiabatic if the system under study (fixed mass) does not exchange heat with its surroundings. In this paper our systems are selected areas or regional boxes, 400 m deep. Thus processes that change the (spatially averaged) temperature of the boxes in question, keeping their mass fixed, are called diabatic processes and those that only produce a change in the mass content (fixed temperature) will be called adiabatic processes.

The main goal of this study is to provide a first, detailed description of the various heat budget components for interdecadal timescales and to offer some speculations about the origin of variability with different timescales using both model and observations. (ENSO-like heat content variability is discussed by *Auad et al.* [this issue] (hereinafter, referred to as part 1).

We find that two dominant timescales occur in the interdecadal band. The first has 10- to 12-year variations that have a prominent adiabiatic response to wind forcing or Rossby wave propagation. The second has a 20-year variation that has a predominantly diabatically driven component. We identify key regions in the Pacific where the model best captures the observed heat content variations and outline the dominant physical balances of processes controlling heat content variations for these two period bands. These fluctuations are then related to the physical mechanisms described in other published model and/or observational studies.

The model and its forcing functions are described in section 2. In section 3 we give a short description of the observations, while in section 4 the methods used to compute heat storages and band pass the data are presented. In section 5 we describe the interdecadal upper ocean heat storage variability, both locally and for regional averages and describe the interdecadal heat budget components, leaving sections 6 and 7 for discussion and summary.

2. The Model

The primitive equation ocean model, known as OPYC (Ocean Isopycnal Model), was developed by *Oberhuber* [1993] and applied by *Miller et al.* [1994ab] to study monthly mean through decadal-scale variations over the Pacific Basin (64°N to 76°S; 120°E to 60°W). The model is constructed from eight isopycnal layers (constant potential density but variable thickness, temperature, and salinity) that are fully coupled to a bulk surface mixed-layer model. The resolution is relatively coarse (4° in the midlatitude open ocean, though with finer resolution near the equator, 0.5° north-south, and 1.6° near the eastern/western equatorial boundaries) so only large-scale patterns can be considered with confidence.

The surface forcing consists of a monthly-mean seasonal cycle climatology of wind stress, total surface heat flux, and turbulent kinetic energy input to the mixed layer, to which are respectively added the specified monthly anomalies estimated for 1970-1988 from the Comprehensive Ocean Atmosphere Data Set (COADS) observations outside the ±20° latitude band. Inside it, COADS and Florida State University (FSU) winds were blended in the following way: FSU data were used in the ±20° latitude band. In an overlap region of approximately 5° latitude at 20°N and 20°S the COADS and FSU anomaly fields were smoothly merged.

Unfortunately, the surface heat flux anomalies are poorly known southward of 20°N owing to poor sampling [e.g., *Cayan*, 1990]. However, it is generally accepted that near the equator (say, within 5° latitudes), surface heat fluxes serve to damp Sea Surface Temperatures (SST) anomalies [*Cayan*, 1990; *Barnett et al.*, 1991] although smaller driving effects can be identified at times, particularly in the western tropical Pacific [e.g., Seager, 1989]. We therefore used a Newtonian relaxation scheme whereby SST anomalies are damped to the model climatology (taken from a seasonal base run) in the region 20°N-20°S. We constructed time series (not shown) of interdecadal surface heat fluxes (National Center for Enviromental Predicition (NCEP) data) and SST (Scripps Institution Joint Environmental Data Analysis Center (JEDAC)) averaged over the eastern and western equatorial Pacific. In both areas, interdecadal surface heat fluxes and SSTs have oppo-

site signs, most of the time (a positive Q meaning a gain of heat for the ocean). This assumption can thus be justified near the equator but cannot be a priori justified for the regions 5N*deg*-20°N and 5°S-20°S; indeed, in these regions the model SST response is poorly matched to observations [*Cayan et al.*, 1995; *Miller et al.*, 1994a] which suggests that heat fluxes are a strong forcing function for SST there. Typical e-folding times, $\rho C_p D/\delta$, range from 20 days (for a 10-m-deep mixed layer) in the western equatorial region to 500 days in the eastern equatorial region (for 100-m-deep mixed layer). Here ρ is the water density, C_p is the constant heat capacity, D is the mixed-layer depth, and δ is the spatially dependent (and very smoothly varying) damping coefficient, whose estimation is described in detail by *Miller et al.* [1994b]. From the point of view of heat content, however, we show that the model closely follows the observations, suggesting that thermocline heave (controlled by wind stress curl or wave propagation) rather than SST variations controls the heat content in these low-latitude subtropical regions.

There is no model feedback of SST to the anomalous heat flux forcing, so that the model is not constrained to reproduce the observed temperature variations. A thorough discussion of the model framework and forcing strategy is provided by *Miller et al.* [1994ab] and *Cayan et al.* [1995]. The forcing strategy was modified from that of *Miller et al.* [1994b] in that we applied the technique of *Killworth* [1996] to properly allow linear interpolation of weighted monthly mean forcing anomalies (added to the seasonal cycle forcing). *Miller et al.* [1994b] did simple linear interpolation of the monthly mean forcing which yields monthly mean model forcing that is typically weaker than the true monthly mean observed forcing. *Killworth* [1996] proposed increasing the input monthly mean forcing fields to allow linear interpolation yet causing the model to properly experience monthly mean forcing from the observations.

The complete model heat budget terms (see section 5.3) were saved as monthly means in each layer of the model. Postprocessing involved summing up the proper fractional number of model layers to determine the heat budget in the upper 400 m of the water column. The heat budget balanced to within 1%. Further postprocessing (filtering, etc.) is discussed in the following sections.

3. The Observations

The temperature data set consists of all available XBT, conductivity-temperature-depth (CTD) and mechanical bathythermograph (MBT) observations over the period 1955-1992 assembled and quality controlled by the JEDAC (http://jedac.ucsd.edu). Processing of the raw hydrographic data to obtain anomalous temperatures at several standard depths from the surface to 400 m is described by *White* [1995]. Since we wish to directly compare the data with a 1970-1988 simulation, we only use data from the 1970-1988 time period which is also the best sampled time interval. A monthly mean climatology was computed for the period 1970-1988, and monthly temperature anomalies were defined with respect to that climatology. Temperature anomalies are then available at a series of standard levels to 400m depth (0 m, 20 m, 40 m, 60 m, 80 m, 120 m, 160 m, 200 m, 240 m, 300 m and 400 m) on a 5° longitude by 2° latitude grid.

4. Methods

Model and observed heat storage were computed by integrating local heat storages in the upper 400 m of the Pacific Ocean,

$$H(x,y,t) = \sum_{z=-400\ m}^{0\ m} \rho_0\ C_p\ T(x,y,z,t)\ \Delta z \qquad (1)$$

where H is heat storage (in Joules per square meter, x, y and z are the east, north, and vertical coordinates respectively; t is time, ρ_0=1025 kg m^{-3} is the reference density and C_p=4180 J kg^{-1} °C^{-1} is the constant heat capacity. T and Δz are the local temperature, and depth interval associated with that temperature respectively (for the model data, Δz is a function of space and time). Observed temperatures are the results of linear interpolation, while model temperatures are the results of layered calculations (with only a fraction of the layer that intersects 400 m included in the evaluation of heat content). Once H is obtained, for both model and observations, the monthly mean climatological annual cycle is removed and the resulting time series band passed in the frequency band of interest.

Separation of interdecadal variations from ENSO-scale variability is important in establishing the controlling physical mechanisms [e.g., *Zhang et al.*, 1997; *Miller et al.*, 1997, 1998]. A band-passing procedure was therefore carried out using the Kaylor filter [*Kaylor* 1977] which has a variable cut off frequency (selected by the user). The filter does not introduce any phase shift in the data and has a remarkable steep cut-off slope. We tested the skill of our filter by computing the cross-spectral analysis between some time series after and before filtering them in the 8-30 y band. In this band the phase and amplitude of the coherence function were always very close to zero (smaller than 20°) and one (between 1.3 and 0.8) respectively and the coherence close to one (higher than 0.83). To further test our band passing filter, we compared band passed time series in the 8-30 y with those filtered in the 8-∞ y band. The resulting time series were very similar so that for this particular case, which has no significant trend and little variance in ultralow frequencies, we can consider these results to be essentially low-passed with an 8-year period cutoff. To test for the stability of the 10-y and 20-y timescales, we band passed the data in different frequency bands (5-y to 25-y; 3-y to 40-y, etc) and ver-

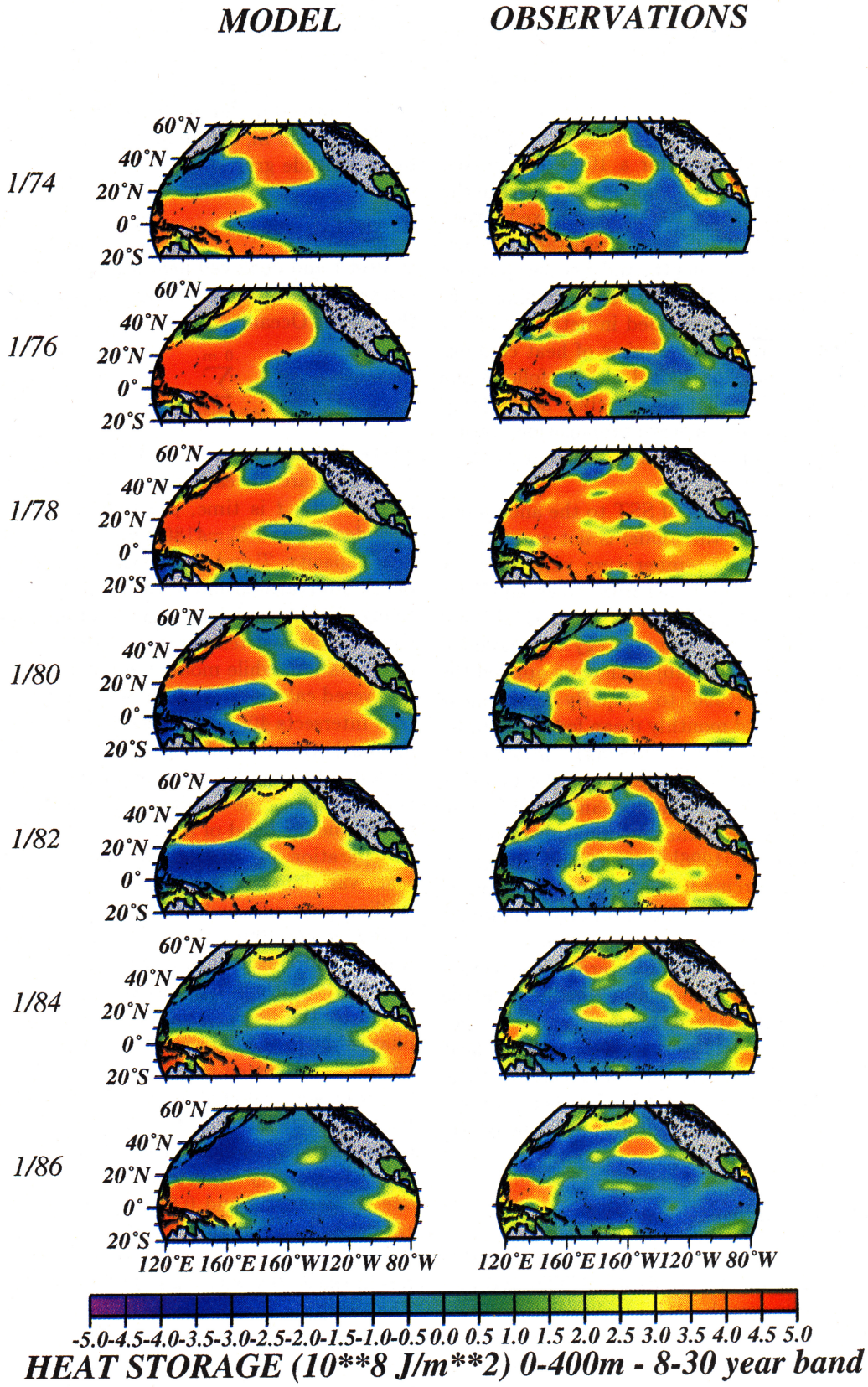

Plate 1. Model and observed heat storage anomalies for interdecadal timescales (8-30 years).

ified that the 10-y and 20-y are present in all cases in the filtered time series.

In this paper, we want to compare our results with the deepest available temperature observations which generally extend to 400 m and that is why we integrate the model temperatures down to 400 m, i.e., to make suitable comparisons with the observed temperature field. In addition, integrating down to 400 m will (1) help to measure the amount of heat exchanged between the upper and deep oceans; (2) include contributions coming from heat fluxes due to turbulent mixing processes characteristic of the mixed layer's base and heat fluxes associated with isopycnal oscillations; (3) allow these results to be compared with those of *White* [1995], who studied many details of the temporal and spatial structure of observed heat storages integrated in the upper 400 m of the North Pacific Ocean; and (4) quantify the contributions to the upper ocean heat content coming from diabatic (fixed mass) and adiabatic (thermocline heave) processes at 400 m.

5. Results

5.1. Modeled and Observed Volume-Integrated Heat Storages

Heat storage anomalies were computed for the period 1970-1988 in the upper 400 m of the Pacific Ocean from both model and observed data. The comparison for unfiltered heat storage is shown in Figures 1a and 1b for the volume north of 24°N and north of the equator, respectively. The former shows a clear dominance of a very low frequency signal in both model and observations, with higher-frequency variations superposed. If the tropics are included (Figure 1b) it is seen that (1) an interdecadal signal is still observed in Figure 1b and (2) the records are better (visually) correlated on timescales of a few years than in the integration performed north of 24°N. This latter comparison motivates the analysis to be presented herein in which the model temperature equation and heat storage time series obtained from historical observations are low passed (8- to 30-year band) for interdecadal timescales. In addition, this analysis is done in different areas or boxes typically 10° by 20° in size and 400 m deep.

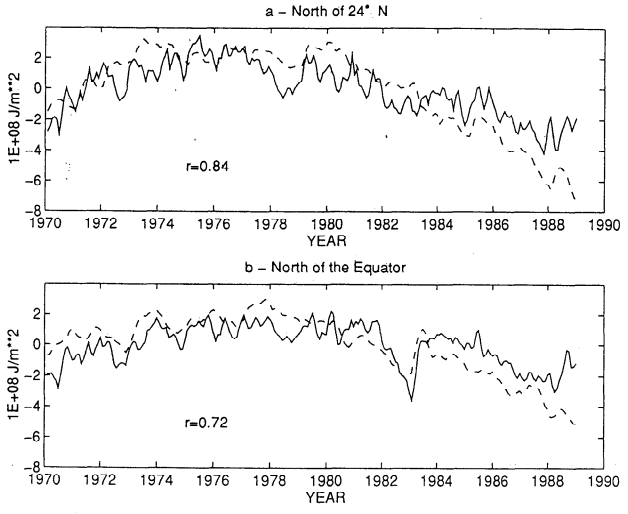

Figure 1. Observed (solid line) and modeled (dashed line) heat storages in the upper 400 m of the North Pacific Ocean averaged for the areas (a) north of 24°N and (b) north of the equator. Zero lag correlation coefficients are also shown

The correlations observed in Figure 1 are bulk estimates of verisimilitude of the model and mix together the large decadal variation with the shorter-timescale fluctuations. Our band-passing technique will be useful in quantifying skill among these dominant frequency bands. The correlations imply that the amount of heat being pumped into or extracted from these volumes, either horizontally or vertically, produces similar changes in the total heat content of the volume for both model and observations. These times series have no information regarding the horizontal distribution of heat storage over the domain under study. This issue is analyzed in section 5.2 by constructing maps of heat storage for interdecadal timescales.

5.2. Modeled and Observed Local Band-Passed Heat Storages

Basic statistical analyses of the band-passed heat storage anomalies were carried out for the time series of each grid point on the respective grids for the model and observed data. The comparisons and analysis are mainly concentrated in the North Pacific Ocean, (NPO) because of its more dense XBT-CTD sampling than the South Pacific. In order to include the whole equatorial band, our maps are constructed from the 20°S parallel northward.

Interdecadal heat storage fields of the upper 400 m from January 1974 to January 1986 every 2 years are shown in Plate 1. In this case, the good agreement between model and observations is more remarkable than for the ENSO timescale (part 1) because anomalous heat storages at interdecadal timescales are rather small and equivalent to temperature changes (in the upper 400 m) of less than 0.1° (≈0.05-0.07°C). The overall picture shows a NPO warming stage from at least 1974 to about 1978, when the upper NPO starts to gradually cool off. This warming-cooling period can also be seen from the volume-integrated heat storages shown in Figure 1. The origin of these changes is not totally clear, but *Miller et al.* [1998] suggest that increased wind stress curl forcing results in a westward intensified raising of the subpolar gyre thermocline in the early 1980s. Anomalous subduction of cold, surface heat flux forced temperature anomalies [*Deser et al.*, 1996] also contributes to the interdecadal cooling observed after 1983 near Hawaii in Figure 1.

These heat storage changes (model and observations) show some evidence for northward propagation of anomalies along the western boundaries into the Kuroshio Ex-

tension as proposed by *Latif and Barnett* [1996], who suggest that a dominant mode (30%) of heat storage interdecadal variability in the North Pacific is influenced by anomalous meridional advection of mean temperature gradients in this region. However, *Miller et al.* [1998] suggest that the subpolar gyre cooling is a stationary response to wind stress curl forcing rather than a propagating response influenced by horizontal advection of cold temperature anomalies. Figure 5b, reveals that the model heat content changes most rapidly in 1975 when meridional advection acts against these changes while thermocline heave, vertical transport processes, and surface heat fluxes drive them. On the other hand, the model heat content changes seen in Figure 5b in 1980 and 1985 are aided by meridional advection, vertical transport, and heave but are opposed by heat fluxes. This complicated and time-dependent balance implies that more than one mechanism is at work during this time period in this region [cf. *Xu et al.*, 1998].

From Figure 1 it can be seen that the first panel bears some similitude to the last one. A longer sequence, not shown (an animation can be seen from the URL address given in section 3) revealed that both model and observed heat storage patterns repeat after about 14 years. The equatorial region shows an interesting eastward propagation of warm anomalies at about the same speed in both model and observations during this time interval. Since the signal requires several years to cross the basin, it is not associated with free Kelvin waves, though the spatial structure mimics El Niño time scale processes. Some minor discrepancies can be seen along the eastern boundary (mainly along the Mexican and California coasts), and this is probably caused by the poor horizontal resolution of coastal processes by the model.

The heat storage anomalies in the upper 400 m of the midlatitude NPO are largely controlled by the lower half of the volume (i.e., 200 m to 400 m, which is generally below the winter mixed layer). In other words, thermocline fluctuations contribute the greatest variations to upper ocean heat content. This suggests that the agreement found in the model-observation comparisons is not simply controlled by model diabatic surface boundary conditions as specified from observations but, rather, by a reasonable simulation of the dynamical contribution to interior heat fluxes. (The reader can make a comparison of heat storage in the upper 400 m versus temperatures at different levels by going to the URL address given previously.)

Correlation coefficients between model and observed heat storages (Figure 2) were computed for interdecadal timescales. The 90% confidence levels were computed according to *Davis* [1976] and are, on a spatial average, 0.7. Areas of highest correlations (Figure 2, light areas), are patchy over the basin but organized by the type of responses known to occur. Unlike the ENSO correlation coefficient map in part 1, in the interdecadal map there are two high-correlation areas located east and south of Japan and one area, eastern equatorial area, showing low correlations (Figure 2, dark areas). Because of the low overall variance levels of decadal-scale variability, low correlation values can be interpreted as, partly, the result of low signal-to-noise ratios. In the low latitudes (20°S to 20°N) the Newtonian heat flux parameterization can explain some of the poorer correlation away from the tropical strip. Also, the data sampling of the low latitudes is sparse and may particularly explain the low correlation found southwest of Central America. Other sources of low correlation can be ascribed to model resolution, unresolved physics, and inadequate forcing data.

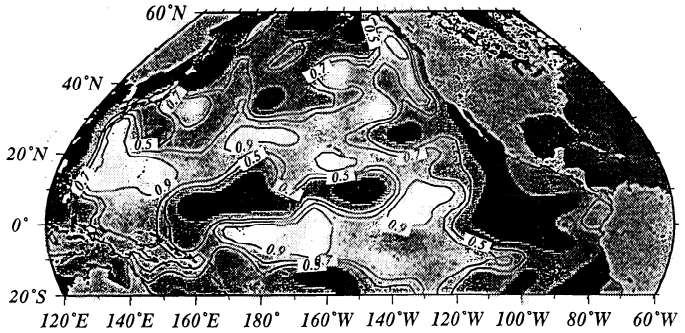

Figure 2. Correlation coefficients between model and observations of heat storage in the upper 400 m for interdecadal timescales. Only the 0.5, 0.7, and 0.9 contours are drawn. The spatially averaged 90% confidence level is 0.7

5.3. Heat Balance in the North Pacific Ocean

5.3.1. Introduction. The heat content of a given volume can change in time owing to changes in the temperature of the water parcels (diabatic) and/or to the arrival and departure of water parcels having a fixed temperature (adiabatic). Since the overall or total heat content can be felt by the overlying atmospheric system, both contributions are studied in detail in this paper. Adiabatic and diabatic heat content changes have their primary origin from different forcing mechanisms, wind stress curl and surface heat flux, respectively. We first describe the overall changes in heat content and the total heat balance and then we study the diabatic contribution to the total heat balance since this is the part of the total heat balance that is directly forced by and interacts with the atmosphere through the net surface heat flux Q. The results are summarized in Table 1.

As in part 1, we analyze here the total heat balance equation, which is defined for each model layer, i.e.,

$$\frac{\partial H}{\partial t} = -\nabla.(\mathbf{V}T\rho hC_p) + VT_{400} + \frac{Q}{D}\delta_{z,0} + H_{mix}, \qquad (2)$$

and the diabatic heat balance equation, i.e.,

Table 1. Dominant Heat Balances and Timescales for the Selected Areas of Figure 3

Area		Dominant Balance	Dominant Timescale years
1,	total	div(VH)=0	8
1,	diabatic	$Q - uT_x - vT_y = 0$	18
4,	total	$H_t = -div(VH)$	10
4,	diabatic	all terms but H_{mix}	10
5,	total	$H_t = -div(VH)$	12
5,	diabatic	all terms	22
7,	total	all terms	10
7,	diabatic	$T_t = -vT_y + Q$	22

Abbreviations are H_t, time derivative of total heat content; Q, net surface heat flux; u and v, zonal and meridional flow speed, respectively; T_x, zonal temperature gradient; T_y, meridional temperature gradient; V, three-dimensional velocity vector; T_t, time derivative of temperature; H_{mix}, horizontal mixing.

$$\rho h C_p \frac{\partial T}{\partial t} = -u\frac{\partial T}{\partial x} - v\frac{\partial T}{\partial y} + V_{mix} + \frac{Q}{D}\delta_{z,0} + H_{mix}, \quad (3)$$

where $\mathbf{V} = (u, v)$ is the velocity vector of each layer with u and v its zonal and meridional components, respectively, and h is the thickness of each layer. From now on, we represent the second term in (2) as div and adv_x and adv_y as the zonal and meridional advection of temperature, i.e., the second and third terms in (3). VT_{400} is the vertical heat transport due to mixing, advection, and divergence, Q is the net surface heat flux and H_{mix} is the horizontal mixing. Note that the words "vertical" and "horizontal" actually mean cross- and along-isopycnal, respectively. If one adds the temperature-weighted mass conservation equation to (3), one can rewrite (2) in the form,

$$\frac{\partial H}{\partial t} = C_p(\rho h\frac{\partial T}{\partial t} + T\frac{\partial \rho h}{\partial t}) \quad (4)$$

which shows the diabatic (second term) and adiabatic (last term) contributions to the total heat balance (first term). For interdecadal scales we found that all analyzed areas have adiabatic/diabatic ratios (the ratio of the standard deviation of the last term to the standard deviation of the second term) between 1 and 1.25.

We now concentrate on those areas where the best agreements between model and observations are found. On the basis of the correlation analysis of the section 5.2, we selected four different areas where the agreement between model and observations is reasonably good. Figure 3 shows three of the regions, while area 7 is the region north of 24°N. These areas were numbered to be consistent with part 1. In these regions, we compare the model and observed heat storages and break down the heat budget of the model. As before, for each area the model and observed heat storages were band passed in the 8- 30-year band (interdecadal timescale) and (1), (2), and (3) are integrated in the upper 400 m and for the areas shown in Figure 3.

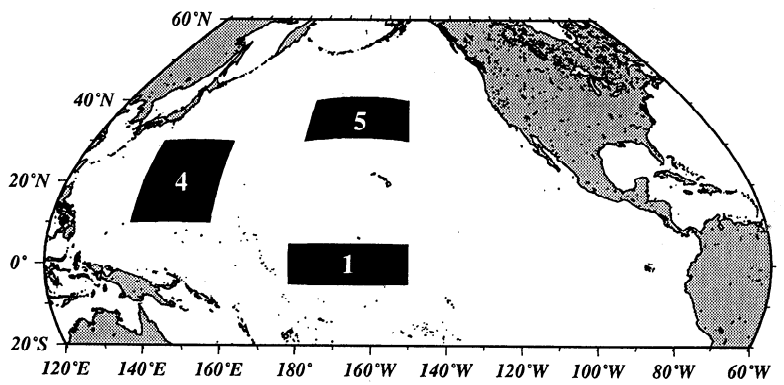

Figure 3. Selected areas where temperatures and heat budget components are averaged

The 400 m depth was chosen because it is the deepest level reached by the observations maintained at JEDAC and it is well beyond the reach of the turbulent effects that characterize the base of the mixed layer. Choosing a fixed reference level, instead of a given isopycnal, is desirable if one wants to study contributions to the heat equation from propagating signals or, more generally, from any motion associated with isopycnal oscillations. We allow these motions to affect (2) since we are interested in providing a complete description of the heat balance that includes all contributions from vertical (oceanic) heat fluxes and also to compare with the 500-m integration *Latif and Barnett* [1996]. To determine how important the contribution from isopycnal oscillations is to (2), we also obtained the heat balance integrated down to layer 4 of OPYC which has bottom depths ranging from 200 to 500 m, depending on the geographical location. The comparison for each box between both vertical integrations gave nearly identical results. This is because the main contribution to heat budget components come from the four upper layers of the model. This implies that we are trapping, in our vertical integrals, the strongest part of the signal in question. The same result was obtained in Part 1 (ENSO timescales). The four different areas were not only chosen because of the high observation-model correlations for heat storage but also because we want to compare some of the present results with those of part 1 and those reported by *Cayan et al.* [1995] and *Miller et al.* [1994a, 1998].

We analyze the total and diabatic heat balance, instead of, say, the diabatic and adiabatic components, because we are interested in the overall or net effect (total balance) and in those changes forced by Q, the net surface heat flux (diabatic balance). Note that even though the diabatic balance is part of the total balance, from (4), see that the descriptions and timescales arising from both balances, total and diabatic, are quite different, in general. The results are summarized in Table 1.

5.3.2. Total heat balance in the North Pacific Ocean. In this subsection we study the total heat balance, $\partial H/\partial t$, as expressed in (2); that is, the joint effects, of both adiabatic and diabatic contributions are taken into account. As mentioned above and for the areas to be considered below, the adiabatic and diabatic components right-hand side in (4)), make comparable contributions. In practical terms, the total heat balance is obtained from the mass conservation and temperature conservation model equations.

Figure 4 shows model and observed box-averaged temperatures band passed in the 8- to 30-year band for four selected areas; western equatorial (area 1), west subtropical (area 4), central north (area 5), and north of 24°N (area 7). The lower correlation obtained in area 2 (eastern equatorial region, not shown) may be due to using a Newtonian heat flux damping mechanism rather than allowing for the possibility that heat fluxes

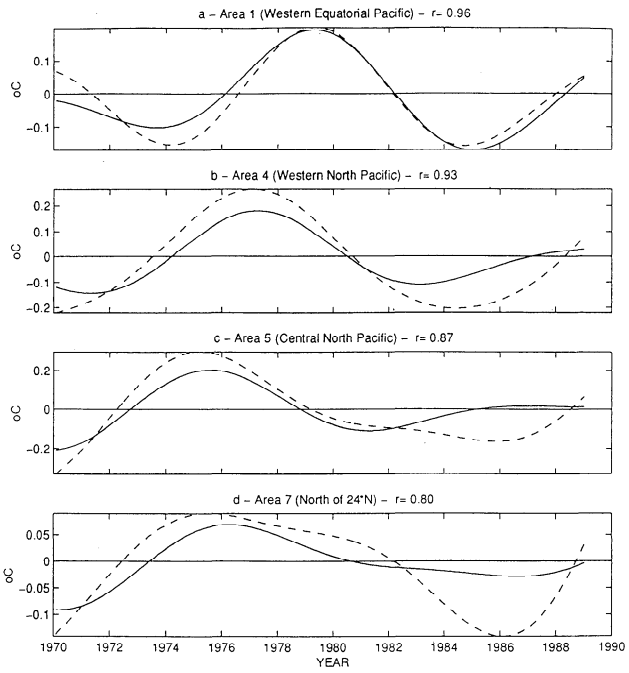

Figure 4. Model (dashed line) and observed (solid line) average box-temperatures for interdecadal timescales in the upper 400 m. Zero lag correlation coefficients are shown at top. Note that different scales are used for each area

drive an interdecadal signal. The low density of observations available in area 3 (10°N-24°N; 170°E-170°W, not shown) can also be degrading the correlation coefficients there. Typical timescales observed in these time series (always for the period 1970-1988) are 11 years for area 1 (western equatorial), 14 years for area 4 (western subtropical), and 22 years for areas 5 (central north) and 7 (north of 24°N). This latter basin-scale timescale, i.e., 22 years, agrees with those reported for the North Pacific by both *Latif and Barnett* [1994] from model data, 20 years, and by *Tourre et al.* [1998] from observations, 23 years, where both studies employed frequency domain EOFs.

It is tempting to try to infer propagation of the signal between areas but travel times are difficult to estimate because the dominant interdecadal mode can only explain 40% of the total variance in that band [*Tourre et al.* 1998]. Thus, the amplitudes of Figure 5 are made up of a superposition of different signals, none individually explaining more than about 40% of the total variance. However, the phase plots of Figure 6 do indicate some westward motion of the heat storage isolines in the interior ocean from 1974-1979 along 30°N, east of 160°E. This motion is at about 3 cm s^{-1} compared with the 5 cm s^{-1} found by *Jacobs et al.* [1994] from sea surface height during the 1980s. However, note that the westward motion in Figure 6 is interrupted by the arrival of warm heat storage anomalies from the south at 150°E that are clearly evident in Plate 1. The mechanisms involved in producing the westward movement

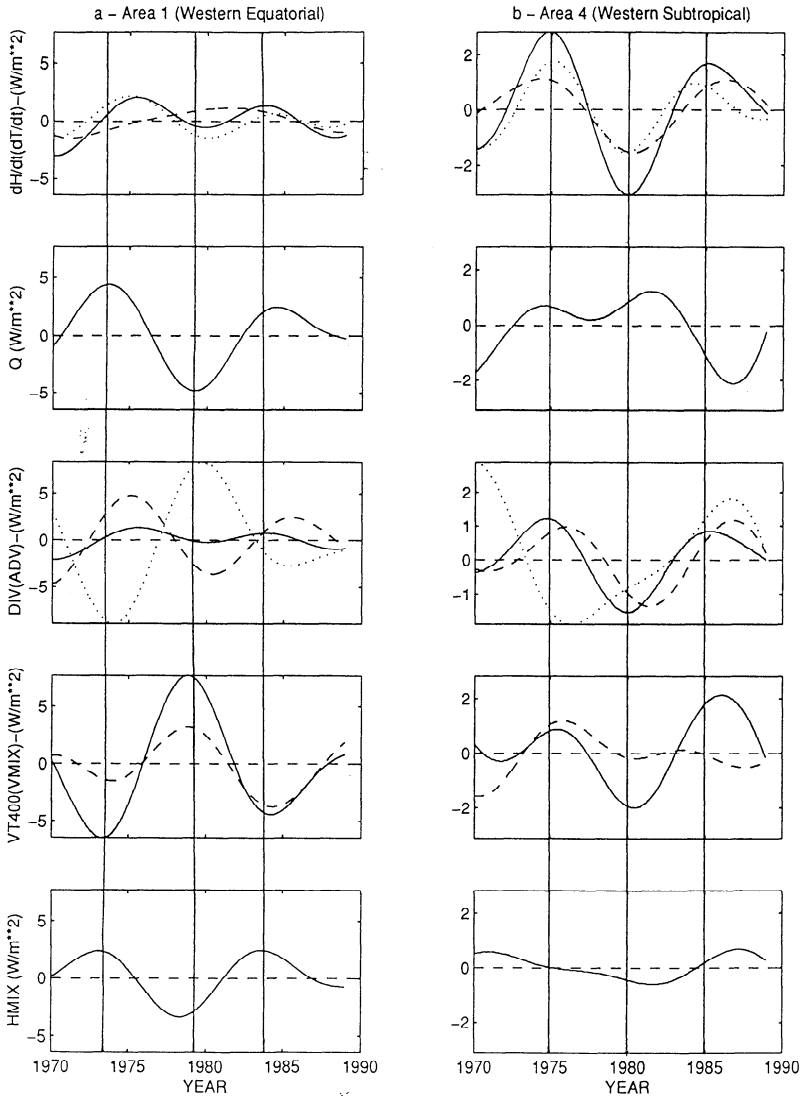

Figure 5. Interdecadal time series of the OPYC temperature and heat equations averaged for areas (a) 1, (b) 4, (c) 5, and (d) 7 shown in Figure 4 and in the upper 400 m. Solid lines are components of the heat equation and dashed and dotted lines are components to the temperature equation. In plots with only the solid curve present it is common to both equations. panels the only curve present (solid) is common to both equations. Here, dH/dt (solid line), dT/dt (dashed line), and $d(\rho h)/dt$ (dotted line), refer to the time change of heat, temperature, and mass, respectively (the last two add up to the first one). Q is the surface heat flux. A positive value implies a gain of heat for the oceanic system. The *div* (solid line) and *adv* (dashed line for zonal advection and dotted line for meridional advection) are the horizontal divergence and the contribution from horizontal advection to that divergence, respectively. VT_{400} (solid line) and V_{mix} (dashed line) are the total vertical heat transport at 400 m (advection plus mixing) and the vertical mixing contribution to that total vertical transport, respectively. In the bottom panel, H_{mix} refers to horizontal mixing and VT_{400} is the vertical heat transport at 400 m. Tt refers to the time derivative of temperature (first term in (2)). Positive and negative values imply warming and cooling, respectively, for the boxes in question

and the northward movement are complicated, however, and not necessarily associated with ocean advection or wave propagation [e.g., *Liu*, 1993; *Liu and Pedlosky*, 1994]. For example, the variations in heat storage seen in Figure 6a can be visually associated with forcing by net surface heat flux Q and the wind stress curl (a positive curl cools the upper ocean). The wind stress curl indirectly enters the heat equation through the VT_{400} (mostly isopycnal displacement). Similar diagrams to the ones of Figure 6 were constructed (not shown) for the heat equation terms. Along 30°N the main balance is between the time change of heat, the vertical transport at 400 m (VT_{400}) and the surface heat flux Q.

Area 1 is located in the western equatorial Pacific,

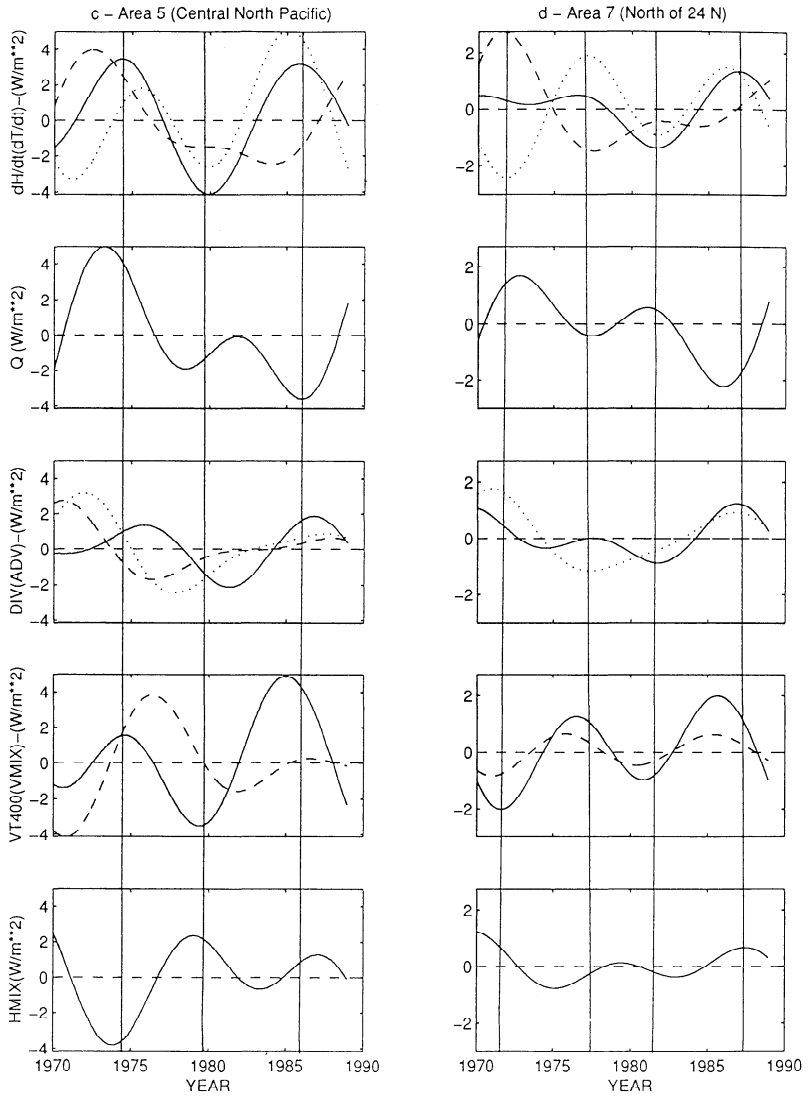

Figure 5. (continued)

and from historical observations it is known that the equatorial strip is characterized by eastward propagating wave activity at both ENSO and longer timescales. The total heat balance for interdecadal timescales in area 1 (Figure 5a) is dominated by Q, the vertical heat transport VT_{400} and horizontal mixing H_{mix}. The local change of heat $\partial H/\partial t$ and the horizontal divergence of the heat flux div) make smaller contributions and tend to cancel each other. Vertical mixing makes an important contribution to the total vertical heat transport VT_{400} until about 1982. From there on it becomes dominant and overcomes the vertical transport of heat due to both advection and divergences (i.e., $w\rho T$, where w is the vertical velocity). Thus this contribution is the total vertical heat transport minus the vertical heat transport due to vertical mixing. From the curves in Figure 5a (top), it is seen that the temporal changes in total heat and its contributions from diabatic sources (first and second terms in (4)) have different timescales. We plotted (not shown) the dashed curve (i.e., diabatic contribution) against the adiabatic contribution, last term in (4), and confirmed that both contributions, adiabatic and diabatic, have different timescales. The adiabatic contribution has a timescale of about 18 year while, the diabatic contribution has a timescale of about 10 year. Unlike the remaining areas to be analyzed, area 1 shows a similar total heat balance for the few events present in the 1970-1988 time span.

Area 4 is located in the center of the NPO subtropical gyre. On several timescales it is characterized by active, wind-induced Ekman pumping which helps to explain why maximum isopycnal depths are observed at this location. The total heat balance for area 4 (western subtropical) is shown in Figure 5b. To a first approximation it could be reduced to one between the time change of heat and the three-dimensional divergence of the heat flux since Q and H_{mix} make smaller contributions and tend to cancel each other for most parts of the record. Unlike the other areas analyzed in this paper area 4 shows similar timescales for both adiabatic and diabatic contributions. In this area, vertical mixing is important and sometimes dominant from 1970

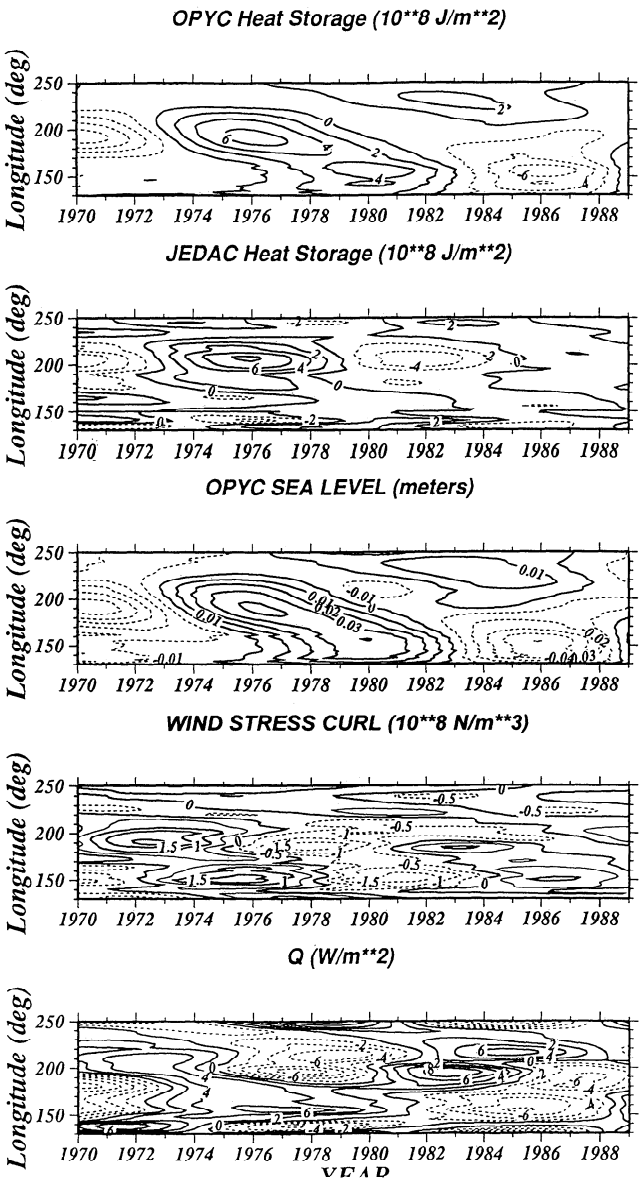

Figure 6. Phase diagrams for heat storage, sea level, wind stress curl, and surface heat flux computed at 30°N

until about 1978 when the total vertical transport of heat VT_{400} starts to be almost entirely dominated by vertical advection and divergences of the heat flux i.e., contributions from $w\rho T$. Following the first and last vertical lines on Figure 5b allows one to compare the two maxima in the time series of the local change of heat. Notice that the total heat balance is not the same for both peaks as Q warms up area 4 in 1975 and cools it off 10 years later.

Area 5 is located in the center of the subtropical NPO, a region occupied by the northern flank of the NPO subtropical gyre. *Cayan et al.* [1995] and *Miller et al.* [1994a] use this same area for describing SST patterns and to compute the mixed-layer anomalous heat budget. Their model SST and heat storage fields (this paper) are highly correlated to SST and heat storage obtained from observations. Figure 5c shows the total heat balance for the central North Pacific region (area 5). Following the vertical lines for the two positive peaks in $\partial H/\partial t$, we can see that the heat balance is not the same one in 1974 when Q warms up and H_{mix} cools off area 5 and in 1986 when the signs of Q and H_{mix} are reversed, despite the fact that area 5 is warming up as in 1974. The timescales of the diabatic (dashed curve in Figure 5c (top)) and adiabatic (difference between the solid and dashed curves) contributions are different. The diabatic contribution has a timescale of about 20- to 24-year while the adiabatic contribution has a timescale of about 9 years. Vertical mixing makes important contributions from 1970 until about 1982, a time when $w\rho T$ starts to control the time series of VT_{400}, the total vertical heat flux crossing the 400-m level.

Area 7 (north of 24°N) is interesting since the current model results can be used (given the high correlations shown in Figure 4) to provide an approximate estimate of the interdecadal timescale to the total meridional heat flux crossing this parallel. The standard deviation of the meridional heat flux normal to the 24°N parallel is 0.62 W m^{-2}. Although the total heat balance for area 7 (Figure 5d) cannot be simplified since all terms make important contributions, the maximum correlations among all terms is between the local change of heat and the horizontal divergence of the heat flux (0.88) and between Q and total vertical transport of heat VT_{400} (-0.84). The heat balance for the two largest positive peaks in $\partial H/\partial t$ (1977 and 1987) are different. In 1982 the local change of heat is balanced by the vertical heat transport at 400 m and by a mild horizontal mixing (Q and div almost cancel each other), while in 1987 the local heat change is the resultant of comparable contributions coming from all the other budget components. As with other areas, the timescales of the diabatic (Figure 5d, top, dashed curve) and adiabatic (difference between the solid and dashed curves) local changes are different; the diabatic contribution has a timescale of about 20-24 years while the adiabatic contribution shows, always in the 1970-1988 period, a timescale of about 9 year (dotted line, Figure 5d, top).

From Figure 5d (middle) it can be seen that the contribution of the meridional advection (the zonal advection is zero) to the horizontal divergence of the heat flux is very important for the period 1970-1984 and dominant after then. Notice also that the time series for the horizontal divergence (solid curve, Figure 5d, middle) shows an oscillation with a 10-year period, which is not present in the meridional advection curve (dashed curve). Thus, 10-year oscillations must be present in the contribution coming from the temperature-weighted divergence of the horizontal mass flux. Vertical mixing makes a contribution to the total vertical heat flux VT_{400} comparable to that one made by $w\rho T$ fluxes.

5.3.3. Diabatic contributions to the total heat balance. The diabatic contribution to the total heat

balance, equation (4), is obtained from the model temperature equation. As can be readily be seen by comparing (2) and (3), it is this equation that is mainly influenced by Q and is not directly related to thermocline heave.

Figure 5a shows the diabatic heat balance for area 1 (western equatorial). Unlike other areas, area 1 has a very small heat content tendency term, so that the horizontal advection of diabatic heat balances surface heat transfers. Area 1 shows a dynamical balance for the major peaks of the Q time series. Cooling from the meridional flow is counterbalanced by both warming from the zonal flow and the surface heat loss (vice versa for the maximum cooling observed in 1979). As for the ENSO timescales (part 1), this area (western equatorial) shows both components of the heat advection term having different signs and similar amplitudes.

The diabatic heat balance for area 4, western subtropical (Figure 5b), is complicated in the sense that all terms, with the exception of horizontal mixing, make important contributions to the total heat budget. Moreover, maximum warming events (Figure 5b, top) do not show the same type of balance at different times. For instance, there is a maximum warming period (in $\partial T/\partial t$) in early 1974 which is balanced by incoming heat from the atmosphere, warming from zonal advection and vertical mixing and cooling from meridional advection. The next positive maximum in $\partial T/\partial t$ occurs in early 1986. It is balanced by cooling through the planes $z = 0$ and z = -400 m, where z is the vertical coordinate, and by heating from both components of the horizontal flow. The maximum cooling period seen in early 1980 shows a balance that seems to be, in general, the mirror image of that described above for the warming episode of early 1986. Note that the meridional advection time series (Figure 5b, dotted line) has a longer timescale than the zonal advection time series.

The diabatic heat balance for the central North Pacific box (area 5) is shown in Figure 5c. All terms, throughout the 19-year long record, present comparable amounts of variability. In general, the surface forcing Q is positively correlated with $\partial T/\partial t$, the local change of diabatic heat. An interesting feature to note is that the amplitude of all terms but Q and $\partial T/\partial t$ seems to decrease after 1982. The two warming events present in our records show the same features: a positive $\partial T/\partial t$, i.e., warming episode, is balanced by warming contributions from the surface forcing and horizontal advection terms. Cooling contributions come from the vertical mixing and horizontal mixing terms. For all areas the typical timescale of the diabatic heat budget components ranges between 10 and 14 years. Both components of the horizontal advection term are about in phase and with similar amplitudes and timescales. These timescales are longer than the ones coming from the horizontal divergence of the mass flux.

For area 7 the dominant diabatic heat balance can be summarized by

$$\rho h C_p \frac{\partial T}{\partial t} = adv_y + \frac{Q}{D}\delta_{z,0} \qquad (5)$$

Figure 5d thus shows that fluctuations in gyre-scale advection through 20°N contribute significantly to the diabatic heat content of the North Pacific. It is interesting to note that meridional advection leads the surface heat fluxes during the warming and cooling trends of the 1970s, suggesting the dynamical instigation of decadal variations. The large cooling event by surface heat fluxes in the mid-1980s does not yield a strong signal in the temperature tendency because of the combined warming effects of meridional advection and vertical processes.

The vertical structure of the interdecadal heat storage signals were compared (not shown) for the tropical and extratropical areas. Interdecadal heat storages were larger than ENSO (part 1) heat storages in midlatitudes and viceversa at tropical locations. In both cases the differences in amplitude between timescales are not bigger than a factor of 2. About 80% of the interdecadal signal, for heat budget components, can be found in the upper four layers of the model (200 m to 500 m) for extratropical heat storages and in the upper two layers (100 to 200 m) for tropical heat storages and tropical and extratropical heat budget components.

6. Discussion

Observed heat content variations are well matched to simulated heat content variations for many regions of the Pacific. We therefore studied the temporal and spatial structure of budget components contributing to heat content variations in key regions of a simulation of the Pacific Ocean.

The local diabatic heat changes for the basin-wide area north of 24°N (a region of interest for the WOCE program) are mainly balanced by the net surface heat flux and meridional advection. The effect of meridional advection has two components, one associated with anomalous currents advecting the mean meridional temperature gradient and one associated with mean advection of anomalous temperature. The latter effect is seen in the observations of *Deser et al.* [1996] and *Zhang and Levitus* [1997] and is invoked by *Gu and Philander* [1997] as a possible oceanic mechanism of extratropical to tropical communication which then couples back to the midlatitudes via the atmospheric bridge [e.g., *Alexander* 1992]. The model does not capture this anomalous subduction process [*Miller et al.*, 1998], however, so according to them, anomalous meridional currents must be considered as the main source of this process in the model.

The area-averaged observed net surface flux Q (i.e., outside the ±20° strip) showed for all the analyzed areas (western subtropical, central north Pacific and north of 24°N) two well-defined timescales characterized by 10- and 20-year fluctuations. These two timescales, seen

here in the interval 1970-1988 are in phase with the spectral peaks in solar irradiance reported by *White et al.* [1997]. They found maximum variability in solar irradiance linked to SST fluctuations in the 8- to 13-year and 18- to 25-year bands. However, these two peaks can also be visually distinguished from band-passed (8-30 year) time series of latent, sensible and latent plus sensible heat flux. The 20-year timescale is seen in the local change of diabatic heat ($\rho C_p \partial T/\partial t$) for all the midlatitude areas except the western subtropical region where the net surface heat flux is represented by a Newtonian damping mechanism. The 20-year fluctuation present in all the subtropical time series of Q is not the only source of 20-year fluctuations seen in the time series of $\rho C_p \partial T/\partial t$ since all subtropical areas have at least one of the heat advection components dominated by a 20-year oscillation. The three-dimensional divergence of the heat flux seems to be entirely dominated by an oscillation with a 10-year long timescale, which is also reflected in the time series of the local change of total heat. On the other hand, the 10-year timescale seen in the time series of the local change of diabatic heat for this same area is probably due to a strong westward advection, i.e., along the southern flank of the subtropical gyre.

Our records were only 19 years long and reference has been made to 10- and 20-year oscillations. Obviously not much statistical significance can be attached to them. However, some ad-hoc confidence can be gained by noting that, (1) their presence in our records is likely an indication of their persistence in time since these two timescales also show up in other research papers (mentioned above) where longer records are used, (2) they are not an artifact of our filtering technique since both timescales can be visually identified from non-filtered records, (3) they are not present at one single location but throughout almost the whole north Pacific which is typical of large scale processes, (4) both model and observations show the same timescales (for heat storage) at different locations. (5) the warm and cold periods observed from Figure 4 agree with what is known about interdecadal variability (e.g., a cooling period starting in the central North Pacific in the early 1980s).

One major difference between the ENSO (part 1) and interdecadal timescales is that for most regions the primary terms in the interdecadal heat balance change with time at a given location. This is because multiple processes contribute to the establishment of different timescales of variability in this period band yielding a broadbanded nature. This may explain the low signal-to-noise ratios reported by *Latif and Barnett* [1994] from model heat storages in the upper 500 m and by *Tourre et al.* [1998] from 20 years of observations in the upper 400 m. Another difference between both timescales is the fact that the adiabatic/diabatic ratios for interdecadal timescales are smaller than for ENSO timescales. This is evidence for a more important role played by the diabatic forcing (surface heat flux) in interdecadal timescales than in ENSO timescales. In most areas of the NPO and for ENSO timescales the net surface heat flux can be eliminated from the heat equation without affecting much the overall budget. This is because much of the heat changes are caused by energetic isopycnal oscillations (adiabatic changes) associated with Rossby waves and direct Ekman pumping displacement of the isopycnals [*Miller et al.*, 1997]. This is not the case in the interdecadal band where Q plays an active role in most regions and also for a basin-scale average.

The results were not sensitive to the choice of depth to which heat content was computed. Almost no changes were observed in the anomalous heat budget when the bottom limit of our vertical integration of the heat budget components was changed from 400 m to a given isopycnal which, depending on the geographical location and time, varies between 200 m (high latitudes) and 500 m (center of the subtropical gyre). The reason for this similarity is given by the fact that the main part of the signals are concentrated in the upper 200 to 300 m of the water column.

7. Summary

The heat content of the upper ocean has a significant impact on the overlying atmosphere on decadal timescales. The total heat content of a given volume varies with time owing to changes in temperature of the water parcels (diabatic effects) and/or the arrival and departure of water parcels having a fixed temperature (the adiabatic effect of thermocline heave). We have therefore sought to identify the spatial and temporal structure of decadal heat content variations and the mechanisms that control them in the North Pacific. We examined model decadal heat storage variations of the upper 400 m of the North Pacific Ocean and showed they agreed well with heat storage observations in the interval 1970-1988.

Table 1 provides an overall summary of the dominant heat balances, both total and diabatic, and associated timescales for the four areas analyzed in this article. The analysis of the total heat balance for the western equatorial region revealed a dominant balance between net surface heat flux, vertical heat transport at 400 m, and horizontal mixing. For the western subtropical Pacific the total heat balance can be reduced, to a first approximation, to one between the total temporal heat change and the three-dimensional divergence. The total balance for the central North Pacific can also be reduced to one between the local heat change and the three dimensional divergence but diabatic and adiabatic temporal heat changes fluctuate independently in time with timescales of 22 and 9 years respectively. The spatial average for the whole north Pacific located north of 24°N showed the same timescales for those contributions, but the total heat balance cannot be simplified since all terms make comparable contributions to the

total heat balance. This latter fact could be related to the low signal-to-noise ratios [*Latif and Barnett* 1994; *Tourre et al.* 1998] found in the North Pacific for heat storages computed in the upper few hundred meters. This suggests that different physical processes, probably with comparable amounts of variance, are present at the same time. Thus, given the spatial complexity of most of the heat equation terms observed at all locations in the North Pacific, a finding also obtained by Latif and *Barnett* [1994], we suggest that a much more detailed analysis of the observations, this model hindcast, and the output of the coupled General Circulation Model (GCM) of Latif and Barnett should be undertaken to more concretely verify which features are of ocean origin and which are forced by the atmosphere.

On interdecadal timescales the midlatitude NPO diabatic heat budget is significantly influenced by meridional advection, so that a three-term approximate balance holds: local change, surface heat flux forcing, and meridional advection. In this area the surface heat flux field has a key role in determining the field of the time change of heat storage in the upper 400 m of the North Pacific, a result also valid for ENSO timescales as noted in part 1. The interdecadal total and diabatic heat balances in the western equatorial Pacific can be approximated by a balance between the horizontal advection, the vertical heat transport at 400 m, and the surface heat flux terms (with zero heat content tendency term). Thus, in tropical areas, the vertical transport of heat at 400 m is not negligible and must be taken into account in order to close the heat balance for interdecadal timescales. This contribution is relevant for future studies aiming to study the heat budget of the deep Pacific Ocean and exchange processes between the upper and deep oceans.

In summary, heat content time series show dominant timescales of about 10-14 years for most regional averages and of about 22 years for basin-scale averages [cf. *Ghil and Vautard*, 1991; Mann and *Park*, 1996]. The 10 year fluctuations were characterized as being more strongly influenced by the adiabatic heat changes (with the exception of the western equatorial region), while the 20-year fluctuations are more strongly influenced by the diabatic fluctuations. This latter timescale is observed in the time series of the net surface heat flux and its components, suggesting the importance of direct thermal forcing of this signal by the atmosphere and the Sun. The 20-year variations are not found in the adiabatic heat budget components. The 10-year timescale is observed in both the net surface heat flux and the adiabatic components (i.e., three-dimensional divergence of the heat flux). The 10-year timescale observed from the surface heat flux is associated with the spectral peak found in the 9- to 13- year band by *White et al.* [1997]. On the other hand, the 10-year timescale noticed in the adiabatic (oceanic) components is linked to strong isopycnal displacements associated with Rossby wave activity and direct forcing by Ekman pumping [e.g., *Jacobs et al.* 1994, *Miller et al.*, 1997].

Remarkable comparisons between model and observed heat storages have been found in spite of the coarse horizontal and vertical resolution of the ocean model. Yet there is much room for improving the model and obtaining more precise estimates of the large-scale processes found in this research. A necessary first step aimed to improve the performance of OPYC is the use of a much finer horizontal grid capable of resolving western boundary currents, coastally trapped waves, and, ultimately, mesoscale variability. This, combined with denser and better observations, will hopefully lead to smaller differences between model and observations and hence to a better understanding of the ocean interior dynamics and its interaction with the overlying atmospheric system.

Acknowledgments. Funding was provided by NOAA under the Scripps Experimental Climate Prediction Center (NA 67 GPO 450), the Lamont/Scripps Consortium for Climate Research (NA 47 GPO 188), and the Paleoclimate Program (NA 66 GP 0274). The National Science Foundation also provided support to A.J.M. under grant OCE97-11265. We also thank the National Space Development Agency of Japan (NASDA) for support under a joint program with JAMSTEC. We thank Dean Roemmich, Josef Oberhuber, and the two reviewers for important comments.

References

Alexander, M. A., Midlatitude atmosphere ocean interaction during El Niño: 1. The North Pacific Ocean, *J. Clim., 9,* 944-958, 1977.

Auad, G., A. J. Miller and, W. B. White, Simulation of heat storages and associated heat budgets in the Pacific Ocean. Part 1. El Niño-Southern Oscillation timescale, *J. Geophys. Res.*, this issue.

Barnett, T.P., M. Latif, E. Kirk and, E. Roeckner, On ENSO Physics, *J. Clim., 4,* 487-515, 1991.

Cayan, D. R., Latent and sensible heat flux anomalies over the northern oceans: Driving the sea surface temperature, *J. Phys. Oceanogr., 22,* 859-881, 1992.

Cayan D., A.J. Miller, T. P. Barnett, N. E. Graham, J. N. Ritchie and, J. M. Oberhuber, Seasonal-to-Interannual fluctuations in surface temperature over the Pacific: effects of monthly winds and heat fluxes, in *Natural Climate Variability on Decade-to-Century Time Scales. National Research Council,* edited by Nat. Acad. Press, Washington DC, 20418, pp. 133-150, 1995.

Davis, R. E., Predictability of sea surface temperature and sea level pressure anomalies of the North Pacific, *J. Phys. Oceanogr., 6,* 249-266, 1976.

Deser, C., M. Alexander and, M. Timlin, Upper ocean thermal variations in the North Pacific during 1970-1991, *J. Climate, 8,* 1840-1855, 1996.

Frankignoul, C., P. Muller and, E. Zorita, A simple model of the decadal response of the ocean to stochastic wind forcing. *J. Phys. Oceanogr., 27,* 1533-1546, 1997.

Graham, N., Decadal scale climatic variability in the tropical and North Pacific during the 1970s and 1980s: Observations and model results. *Clim. Dyn., 10,* 135-162, 1994.

Ghil, M., and, R. Vautard, Interdecadal oscillations and the

warming trend in global temperature time series. *Nature, 350,* 324-327, 1991.

Gu, D., and, S.G. Philander, Interdecadal climate fluctuations that depend on exchanges between the tropics and extratropics. *Science, 275,* 805-807, 1997.

Jacobs, G.A., H.E. Hurlburt, J.C. Kindle, E.J. Metzger, J.L. Mitchell, W.J. Teague and, A.J. Wallcraft, Decade-scale trans-pacific propagation and warming effects of an El Niño anomaly, *Nature, 370,* 360-363, 1994.

Jin, F.-F., A theory of interdecadal climate variability of the North Pacific ocean-atmosphere system, *J. Clim., 10,* 1821-1835, 1996.

Kaylor R. E., Filtering and decimation of digital time series, *Tech. Rep. BN 850,* 42 pp., Institute for Physical Science and Technology, University of Maryland, 1977.

Killworth, P., Time interpolation of forcing fields in ocean models, *J. Phys. Oceanogr., 26,* 136-143, 1996.

Latif, M. and, T. Barnett, Causes of decadal climate variability over the North Pacific and North America, *Science, 266,* 634-637, 1994.

Latif, M., and, T. Barnett, Decadal climate variability over the North Pacific and North America - Dynamics and predictability, *J. Clim., 9,* 2407-2423, 1996.

Liu, Z., Thermocline forced by varying wind: Spin-up and spin-down, *J. Phys. Oceanogr., 23,* 2505-2522, 1993.

Liu, Z., and, J. Pedlosky, Thermocline forced by annual and decadal surface temperature variation. *J. Phys. Oceanogr., 24,* 587-608, 1994.

Mann, M.E., and, J. Park, Joint spatiotemporal modes of surface temperature and sea level pressure variability in the northern hemisphere during the last century, *J. Clim., 9,* 2137-2162, 1996.

Miller, A.J., D.R. Cayan, T. P. Barnett, N. E. Graham and, J. M. Oberhuber, The 1976-77 climate shift of the Pacific Ocean, *Oceanography, 7,* 21-26, 1994a.

Miller, A.J., D.R. Cayan, T. P. Barnett, N. E. Graham and, J. M. Oberhuber, Interdecadal Variability of the Pacific Ocean: model response to observed heat flux and wind stress anomalies, *Clim. Dyn., 9,* 287-302, 1994b.

Miller A. J., W. B. White and, D. R. Cayan, North Pacific Thermocline Variations on ENSO timescales, *J. Phys. Oceanogr., 27,* 2023-2039, 1997.

Miller A. J., D. R. Cayan and, W. B. White, A westward-intensified decadal change in the North Pacific thermocline and gyre-scale circulation, *J. Clim.*, in press, 1998.

Oberhuber J. M., Simulation of the Atlantic circulation with a coupled sea ice - mixed layer isopycnal general circulation model. Part I: model description and part II: model experiment, *J. Phys. Oceanogr., 23,* 808-845, 1993.

Robertson, A.W., Interdecadal variability over the North Pacific in a multi-century climate simulation, *Clim. Dyn., 12,* 227-241, 1996.

Seager, R., Modeling tropical Pacific sea surface temperature: 1970-1987, *J. Phys. Oceanogr., 19,* 419-434, 1989.

Tourre, Y. M., Y. Kushnir, and, W. B. White, Evolution of Interdecadal Variability in SLP, SST and Upper Ocean Temperature over the Pacific Ocean, *J. Phys. Oceanogr.*, in press, 1998.

Trenberth, K. E., Recent observed interdecadal climate change in the Northern Hemisphere, *Bull. Amer. Meteor. Soc., 71,* 988-993, 1990.

White W. B., Design of a global observing system for gyre-scale upper ocean temperature variability, *Progress in Oceanography, 36,* 169-217, 1995.

White, W. B. and, C-K. Tai, Inferring interannual changes in global heat storage from TOPEX altimetry, *J. Geophys. Res., 100,* 24943-24954, 1995.

Xu, W., T.P. Barnett, and, M. Latif, Decadal variability in the North Pacific as simulated by a hybrid coupled model, *J. Clim.*, in press, 1998.

Zhang, R.-H. and, S. Levitus, Structure and cycle of decadal variability of upper ocean temperature in the North Pacific, *J. Clim., 10,* 710-727, 1997.

Zhang, Y., J. M. Wallace and D. S. Battisti, ENSO-like interdecadal variability: 1900-93, *J. Clim., 10,* 1004-1020.cGraw-Hill, N.Y., 1962. McGraw-Hill, N.Y., 1962.

G. Auad, A. Miller, and W. White, Climate Research Division, Scripps Institution of Oceanography, University of California, San Diego, 9500 Gilman Dr., La Jolla, CA 92093. (e-mail: guillo@ucsd.edu)

(Received June 18, 1997; revised April 2, 1998; accepted June 16, 1998.)